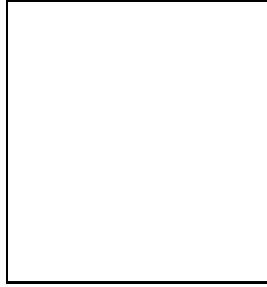


# PIERRE AUGER OBSERVATORY STATUS AND RESULTS

V. VAN ELEWYCK

for the Pierre Auger Collaboration

*Institut de Physique Nucléaire d'Orsay, Université de Paris Sud & CNRS-IN2P3  
15, rue G. Clemenceau, 91406 Orsay Cedex, France*



The Pierre Auger Observatory, a hybrid detector for the study of ultra-high energy cosmic rays (UHECRs), is now approaching completion. After describing Auger present status and performance, with an emphasis on the advantages provided by the combination of two different detection techniques, this contribution presents a brief panorama of the first scientific results achieved and of their impact on our knowledge of the UHECRs' origin and composition.

## 1 Introduction

Despite the important progress achieved in cosmic ray physics during the last decades, fundamental questions about the nature and origin of the ultra-high energy cosmic rays (UHECR) are still unanswered. Contradictory results<sup>1,2</sup> have been reported about the presence of the expected GZK cutoff in the cosmic ray spectrum at energies around  $5 \times 10^{19}$  eV; and the identification of possible acceleration sites still awaits the observation of an unambiguous correlation of UHECR with astrophysical objects (see<sup>3</sup> for recent reviews on these issues). The Pierre Auger Observatory<sup>4</sup> is expected to shed some light on these longstanding questions. Its hybrid design, combining a surface detector (SD) and a fluorescence detector (FD), makes it sensitive to different - and complementary - observables of the extensive air showers (EAS) related to the primary UHECR properties. With more than 75% of the SD stations deployed and all four fluorescence telescopes operational at the time of writing, the Auger Southern Site (located in the province of Mendoza, Argentina) is now nearing completion and has been accumulating high-quality data at a regularly increasing pace for the past three years. After a brief description of the detector and its current performance in Sec. 2, a review of the significant physics results already produced by Auger concerning the UHECR energy spectrum (Sec. 3), arrival directions (Sec. 4) and composition (Sec. 5) will be presented.

## 2 Status and description of the observatory and its dataset

The SD is a triangular array of 1600 water tanks distant 1.5 km from each other, which sample the shower content at ground. The Cherenkov light emitted by the particles entering the tank is detected by three photomultipliers and the corresponding signals are digitized at 40 MHz by Flash Analog-Digital Converters (FADC). Two local triggers are used: a simple “Threshold” (Th) one, and a “Time-over-Threshold” (ToT) one which requires a lower but more extended signal (at least 12 FADC bins) and is more sensitive to the electromagnetic (EM) component of the shower. A global trigger (T3) then asks for a relatively compact configuration of local triggers compatible in time with the arrival of a shower front. Finally, offline criteria are applied to reject accidental triggers (“physics trigger”, T4) and to ensure the reconstructibility of the events (“quality trigger”, T5)<sup>5</sup>. The SD is constantly active and provides the bulk of data required for high-statistics analysis. Its detection efficiency is 100 % above  $10^{18.5}$  eV at zenith angles below  $60^\circ$ . The angular accuracy on the arrival direction is determined on the basis of an empirical model for the time measurement uncertainties<sup>6</sup>; it depends on the number of hit stations but is always better than  $2^\circ$  for events at  $\theta \leq 60^\circ$ .

The SD array is overlooked by four FD sites that measure the ultraviolet light produced when charged particles in the air shower excite nitrogen molecules in the atmosphere. Each site features six Schmidt telescopes that cover a field of view of about  $30^\circ \times 30^\circ$  each. The signal is collected on a 440 pixels camera and digitalized at a 100 MHz sampling rate. The fluorescence light emitted by the shower is roughly proportional to the energy dissipated in the atmosphere. The fluorescence telescopes can be used only during dark, moonless nights, which reduce their duty cycle to about 14%. The timing and position of the triggering pixels allow to reconstruct the shower-detector plane with an accuracy of about  $0.3^\circ$ , but the uncertainty on the orientation of the shower axis within that plane is much larger.

Most events seen by the FD also trigger at least one SD station, and the additional timing information allows to significantly improve the accuracy both on the reconstructed arrival direction ( $\sim 0.5^\circ$ ) and the position of the core ( $\sim 50$ m). These *hybrid* events amount to about 10% of the total data sample; they allow to fully exploit the detector capabilities and therefore have an important impact on many analysis performed on Auger data. High-quality events, which independently trigger the FD and the SD and can be successfully reconstructed by both detectors, are tagged as *golden hybrids*. These events allow the simultaneous measurement and cross-calibration of different shower parameters related to the energy and nature of the UHECRs. Such a strategy allows to extract physical information about their spectrum and composition while minimizing the dependence in model assumptions, as will be illustrated in the next sections.

## 3 The spectrum of UHECR

### 3.1 General strategy

The key ingredients for the determination of the UHECR spectrum are the accurate determination of the primary energy, which is best achieved with the fluorescence technique, and a large and easily calculable exposure, which is provided by the SD.

The signals in the triggered stations are used to reconstruct both the shower core position and its lateral profile at ground. The parameter  $S(1000)$ , *i.e.* the signal that would be produced in a tank located at 1000 m from the shower core, is measured with an accuracy better than 12% and can be used as an estimator of the size (and thus energy) of the shower<sup>8</sup>. For a given energy, its value depends on the zenith angle of the shower as a consequence of geometrical effects and of the attenuation of the shower in the atmosphere. The “constant intensity cut” method<sup>7</sup> is used to extract the shape of this attenuation curve,  $CIC(\theta)$ , from the data assuming

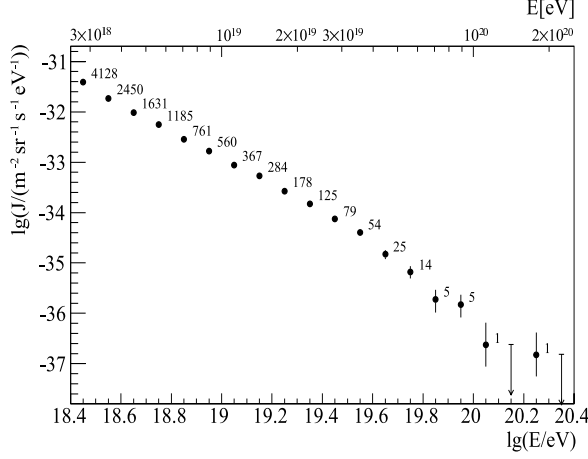


Figure 1: Auger spectrum  $J$  in function of the energy (with the number of events per bin), obtained from the SD dataset as described in Sec.3.1. Vertical error bars are statistical only. Stat. and syst. errors in the energy scale are  $\approx 6\%$  and  $\approx 22\%$  (from <sup>10</sup>).

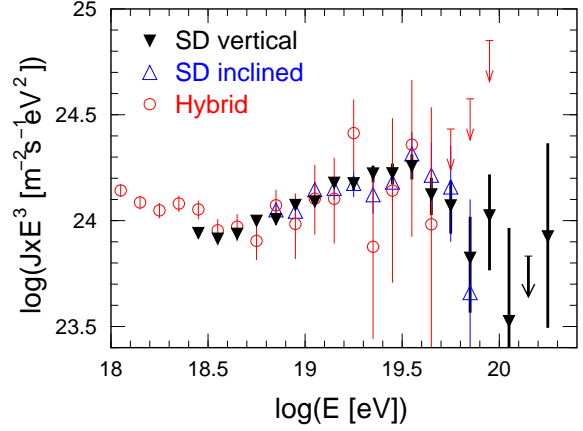


Figure 2: Comparison of that spectrum (labeled SD vertical) with the spectra obtained from hybrid events (Hybrid) and from inclined SD events (SD inclined), all multiplied by  $E^3$  (from <sup>10,13,15</sup>).

an isotropic flux of UHECRs. The  $S(1000)$  is then converted into a reference value taken at the mean of the zenith angle interval,  $S_{38^\circ} \equiv S(1000)/CIC(\theta)$ .

The relation of  $S_{38^\circ}$  (or  $S(1000)$ ) to the primary energy however significantly depends on the assumptions on the primary composition and on hadronic models which drive the development of the shower. This drawback is circumvented by using the golden hybrid events to calibrate  $S_{38^\circ}$  on the energy obtained with the FD. The information on the shower longitudinal profile provided by the FD indeed allows an independent, nearly-calorimetric measurement of the energy of the shower,  $E_{FD}$ . Dependence in composition and hadronic models only affects the determination of the *invisible* component, *i.e.* muons and neutrinos, which contributes only 4% of the total uncertainty in the FD energy. More significant sources of systematics are the uncertainty on the fluorescence yield and its dependence in the atmospheric conditions, the absolute calibration of the FD and the energy reconstruction method. Current estimations<sup>9</sup> of the overall systematics in  $E_{FD}$  give about 22%, while the statistical uncertainty in the derived energy is smaller than 10%.

The dataset now used to build the spectrum includes all SD T5 events recorded between January 1st, 2004 and February 28th, 2007, with reconstructed  $\theta \leq 60^\circ$  and energy  $E_{FD} \geq 3$  EeV, which ensures full detection efficiency of the SD and allows a geometrical computation of the corresponding aperture. After removal of periods of failure in data acquisition, the corresponding integrated exposure amounts to about  $5165 \text{ km}^2 \text{ sr yr}$ , which is more than three times the one obtained by the AGASA experiment<sup>1</sup>. The corresponding spectrum is shown in Fig. 1 together with its statistical uncertainty. Although the statistics is still limited, the hypothesis of a continuation of the UHECR spectrum in the form of a pure power law beyond  $10^{18.6} \text{ eV}$  can now be rejected at a  $6\sigma$  confidence level, as discussed in <sup>11</sup>. Efforts to reduce the systematics in the energy estimation are in progress as well. In particular, recent and ongoing measurements<sup>12</sup> of the fluorescence yield at a precision level of 5% are expected to significantly improve the accuracy in the reconstructed  $E_{FD}$ .

### 3.2 Spectrum from inclined events

The use of Cherenkov water tanks as surface detectors allows the Auger to detect showers with zenith angles up to  $90^\circ$  (and even beyond). The range of inclined showers,  $60^\circ \leq \theta \leq 90^\circ$ ,

contributes half the total solid angle of the detector and about 25% of its geometrical acceptance, thereby significantly increasing the field of view of the detector and the SD statistics.

Such showers are characterized by a dominance of the muonic component at ground and by a very elongated and asymmetrical footprint which can exhibit a lobular structure due to the bending action of the geomagnetic field. The energetic (10 – 1000 GeV) muons reach the detector in a thin front with small curvature, which produces short and peaked FADC pulses. Dedicated selection procedures and reconstruction methods, based on the use of density maps of the number of muons at ground, have been developed to analyze such events; more detail can be found in <sup>14</sup>.

The strategy for building a spectrum is the same as in Sec. 3.1. Once the arrival direction is reconstructed, the pattern of signals is fitted to muon density maps obtained from simulated proton showers at  $10^{19}$  eV in order to determine the core position and an overall normalisation factor,  $N_{19}$ , which acts as an energy estimator and can be calibrated on the FD energy using inclined hybrid events. No constant intensity cut is needed because the muon maps already account for the shower attenuation and geometrical effects. Inclined events with  $60^\circ \leq \theta \leq 80^\circ$  and  $E_{FD} \geq 6.3$  EeV ( $N_{19} \geq 1$ ), where the SD detection efficiency is expected to be 100%, have been used to build this independent spectrum <sup>15</sup>. The corresponding integrated exposure amounts to 1510 km<sup>2</sup>syr, about a quarter of that of "vertical" ( $\theta \leq 60^\circ$ ) events.

### 3.3 Spectrum from hybrid events

Although their statistics is much smaller, hybrid events alone allow a spectrum determination below the energy threshold of the SD <sup>13</sup>. To guarantee the quality of the reconstruction, only events with a reconstructed  $\theta \leq 60^\circ$  and satisfying extra requirements on the observed profile were selected. In particular, the contamination by Cherenkov light may not exceed 50% and the reconstructed depth of the shower maximum,  $X_{max}$ , must be observed and lie within a fiducial volume (which depends on the energy) in order to avoid biases due to the limited field of view.

The hybrid exposure is estimated on basis of a detailed Monte Carlo simulation which accounts for the growth of both FD and SD during the data taking period, as well as for seasonal and instrumental effects. The hybrid trigger efficiency reaches 100% at  $10^{18}$  eV, independently of the nature of the primary (proton/iron). The main sources of uncertainty again lie in the determination of the energy (and its impact on the event selection and aperture calculation), the knowledge of atmospheric conditions and the estimation of the detector uptime; see <sup>13</sup> for a more detailed discussion.

The three spectra (multiplied by  $E^3$ ) are compared in Fig. 2. The spectrum from SD vertical events is the most accurate and statistically significant. The hybrid spectrum extends to lower energies and encompasses the "ankle", which appears as a spectral break at  $\sim 10^{18.5}$  eV. A detailed assessment of the sources of systematics remains to be done for inclined events, but all three spectra are in reasonable agreement within current estimated uncertainties.

## 4 The arrival direction of UHECR: anisotropy searches

Anisotropies in the flux of UHE cosmic rays may appear in different energy ranges and angular scales, depending on the nature, distance and extension of the source(s). Cosmic rays around an EeV are thought to be of galactic origin, and the region of the Galactic Center (GC) and the Galactic Plane (GP) are key targets for anisotropy searches performed with Auger data in that energy range. At higher energies one rather expects UHE cosmic rays to come from extra-galactic sources; a search for directional excesses of cosmic rays could then reveal a correlation with astrophysical objects or even exotic sources.

The anisotropy studies performed by Auger are based on both SD T5 and hybrid events with  $\theta < 60^\circ$  and the energy assigned via the cross-calibration procedure described in Sec. 3.1.

#### 4.1 Anisotropy studies around the Galactic Center and the Galactic Plane

In the past, two cosmic ray experiments, AGASA and SUGAR, have claimed significant excesses in the flux of UHECR in the region of the GC<sup>16,17</sup>. Recent TeV  $\gamma$ -ray observations by HESS<sup>18,19</sup> have provided additional hints towards the presence of powerful CR accelerators in the Galaxy. In that context, several models that predict a detectable flux of neutrons from the GC in the EeV range (when the neutron decay length is about the distance from the GC to the Earth) have also been proposed<sup>20</sup>.

With the GC well in the field of view and a much better angular resolution than previous CR experiments, the Pierre Auger Observatory is well suited to look for UHECR anisotropies coming from that region. Such a search was performed on the bulk of SD data in different energy ranges and with different sizes of the angular filtering in order to match the resolution of previous experiments. Using a data sample much larger than the AGASA and SUGAR ones (79265 SD events and 3934 hybrid events with  $\theta \leq 60^\circ$ ,  $10^{17.9} \text{ eV} < E < 10^{18.5} \text{ eV}$ , corresponding to the period from January 2004 to March 2006), Auger did not confirm any of the anisotropy claims<sup>21</sup>.

The same data were also used to search for a point source in the direction of the GC itself at the scale of Auger's own angular resolution<sup>21</sup>. Applying a  $1.5^\circ$  Gaussian filter to account for the pointing accuracy of the SD, no excess of events was observed. Assuming both the source and the bulk CR at those energies have a spectrum index of 3.3 and that the emitted CRs are protons, an 95% C.L. upper limit of  $\Phi_s^{95} \leq \xi \cdot 0.13 \text{ km}^{-2} \text{ yr}^{-1}$  (where  $\xi$  parameterizes the uncertainties on the flux normalization) is set on the source flux<sup>a</sup>.

A recent update of this analysis with a better angular accuracy and a significantly larger dataset allowing to split the energy range in  $0.1 \text{ EeV} \leq E \leq 1 \text{ EeV}$  and  $1 \text{ EeV} \leq E \leq 10 \text{ EeV}$  have confirmed all negative anisotropy results and improved the bound on  $\Phi_s^{95}$  to  $\xi \cdot 0.018 \text{ km}^{-2} \text{ yr}^{-1}$ . Such a limit already excludes most of the models of neutron production at the GC<sup>22</sup>.

Finally, several methods have been set up to search for large-scale anisotropies in the distribution of UHECR at energies around the EeV (and above); such angular patterns would hint towards a galactic origin of the UHECR just below the ankle. With the current data set, the right ascension distribution is found to be compatible with an isotropic sky<sup>23</sup>. Searches for bidimensional patterns, such as a possible dipole, are also ongoing.

#### 4.2 Searches for localized excesses and correlations with astrophysical objects

Blind searches using Auger data have been performed looking for small- and intermediate-scale excesses in the sky that would reveal the presence of point-like sources. The statistical significance of such an excess is estimated by calculating the two-point angular correlation function, which counts the number of pairs of events with energy larger than a given threshold  $E_{th}$  separated by less than an angle  $\theta$ . Recent studies on SD T5 data with  $E > 10 \text{ EeV}$ , scanning a large range of  $(\theta, E_{th})$ , shows no really significant signal of anisotropy, although some hints of clustering exist at very high energies and intermediate angular scale<sup>24</sup>.

Events with energies above 10 EeV have also been used to test a possible correlation with subsets of BL Lacs, in relation with previous (and sometimes contradictory) claims and results based on data from AGASA, Yakutsk and HiRes experiments<sup>25</sup>. With 6 times more events than the other existing data samples, the analyzed Auger data is still compatible with isotropy and does not support any of the previously reported signals of clustering.

---

<sup>a</sup>This bound could however be about 30% higher if the CR composition at EeV were heavy.

Anisotropy searches based on Auger list of prescribed targets with definite angular and energy windows as released in <sup>26</sup> has also given negative results. As more data is streaming in, the catalogue of candidate targets that will be studied is expected to increase in the future.

## 5 The nature of UHECR: composition studies

Thanks to its hybrid design, Auger can in principle measure an extended set of parameters sensitive to the primary UHECR nature and mass. While the discrimination between different types of nuclei is complicated by the uncertainties in the hadronic models, several methods have already been proposed for the identification of photon and neutrinos. The detection of such particles in the UHE cosmic radiation would probe many exotic models of UHECR production and help locate candidate sources as they travel undeflected by the ambient magnetic fields.

### 5.1 Upper limit on the flux of UHE photons

Unlike protons and nuclei, the development of photon showers is driven by electromagnetic (EM) interactions and does not suffer much from the uncertainties in hadronic models. Their development is also delayed due to the small multiplicity in EM interactions and to the LPM effect <sup>27</sup>, which reduces the bremsstrahlung and pair production cross-sections above 10 EeV.

One of the methods set up by Auger to identify photon primaries in the flux of UHECR is based on the direct observation of the longitudinal profile of the shower by the FD; the discriminating variable is the atmospheric depth of the shower maximum,  $X_{max}$  (the estimated average difference in  $X_{max}$  between photons and hadrons is about 200gr/cm<sup>2</sup>). The data set used for this analysis are hybrid events with a reconstructed energy  $E > 10^{19}$  eV registered between January 2004 and February 2006. A series of cuts were applied to guarantee the quality of the hybrid geometry and of the fit to the shower longitudinal profile (which takes into account the local atmospheric conditions), and to minimize the bias against photons introduced in the detector acceptance by requiring the  $X_{max}$  to be inside the field of view. For all (29) events passing the cuts, the observed  $X_{max}$  is well below the average value expected from the simulation of 100 photons showers in the same conditions. Taking systematic uncertainties on the  $X_{max}$  determination and the photon shower simulations into account, this analysis, described in <sup>28</sup>, allowed to put a 95% C.L. upper limit on the photon fraction of 16% above 10 EeV; it has been recently updated to 13% using a more extended data sample <sup>29</sup>, as shown in Fig. 3.

Another analysis relying on the SD measurements has also been developed; the key observables are here the signal risetime at 1000 m (*i.e.* the time it takes for the signal to rise from 10% to 50%) and the radius of curvature of the shower front. Particles from showers with a larger  $X_{max}$  (and thus a later development) are indeed expected to reach the ground in a thicker and more curved front. A principle component analysis combining both observables was used to search Auger data for photons; no candidate was found and the corresponding upper limit on the photon fraction is 2.0%, 5.1% and 31% at 10, 20 and 40 EeV respectively.

As shown in Fig. 3, the stringent limits put by Auger results on the UHE photon fraction now disfavour many of the top-down models proposed in connection with the AGASA spectrum.

### 5.2 Upper limit on the flux of UHE neutrinos

Due to their small interaction cross-section, neutrinos can penetrate large amounts of matter and generate showers at any atmospherical depth, unlike protons or photons. Young and deep neutrino-induced showers can thus be efficiently identified in the range of inclined showers,  $\theta \geq 60^\circ$ , by requiring the presence of a significant EM component.

Upward-going tau neutrinos that graze the Earth just below the horizon could also be detected as they are likely to interact in the crust and produce a tau lepton which may emerge and

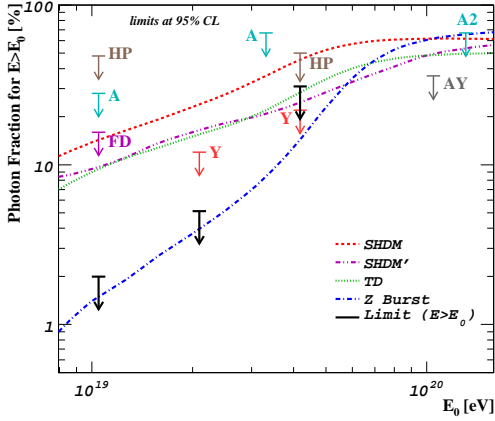


Figure 3: Auger upper limits on the UHE photon fraction from the hybrid analysis (labeled FD) and from SD analysis (black arrows), together with some predictions from top-down models and the bounds put by previous experiments (from <sup>29</sup>).

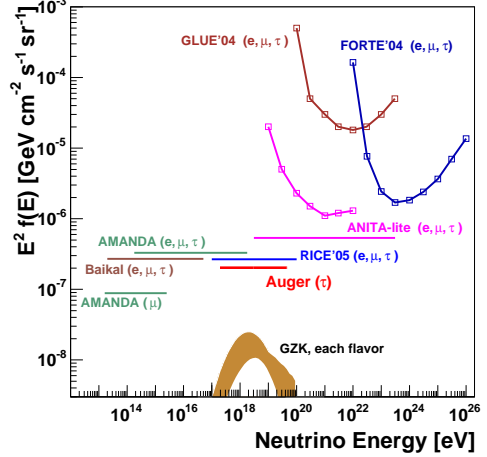


Figure 4: Auger upper limit on an  $E^{-2}$  diffuse flux of UHE  $\nu_\tau$  (with the worst estimation of systematics), together with some predictions for GZK neutrino fluxes and the bounds put by other cosmic neutrino experiments (from <sup>33</sup>).

initiate an observable shower, provided it does not decay too far from the ground<sup>30</sup>. This channel had been pointed out as likely to increase the detection potential of Auger SD for neutrinos in the EeV range<sup>31</sup>; an extensive study has now been performed on the available data<sup>32,33</sup>.

The emerging  $\tau$  flux corresponding to a given incident  $\nu_\tau$  flux has been computed in the relevant angular window using both Monte Carlo and semi-analytical methods accounting for all  $\nu_\tau \longleftrightarrow \tau$  conversion processes, as well as for the  $\tau$  energy losses. The atmospheric shower produced by the decay of the emerging  $\tau$  is then simulated and tested for detection in the SD.

A specific selection procedure has been set up to identify those  $\tau$ -induced, nearly horizontal showers that develop close to the detector. The signal shape must be compatible with the presence of a significant EM component (in practice a ToT-type trigger is required) and a large ( $> 1.4$ ) area-to-peak ratio to reject triggers produced by consecutive muons. The footprint of those stations is then required to assume an elongated shape and the timings to be compatible with a shower front traveling nearly horizontally at the speed of light. The efficiency of identification of a  $\tau$ -induced shower depends on  $E_\tau$  and on  $h_c$ , the altitude of the shower center (defined at a nominal distance of 10 km from the  $\tau$  decay point along the shower axis), but also on the relative position of the footprint in the array. To compute the detector acceptance for  $\nu_\tau$ , a double Monte Carlo integration accounting for the evolution of the array with time is performed.

SD data from January 2004 till December 2006 were searched for candidate grazing  $\nu_\tau$ 's, but no single event passed the selection criteria, which allows to derive an upper limit for any injected flux of UHE  $\nu_\tau$  with a given shape. Assuming an  $E^{-2}$  incident spectrum of diffuse  $\nu_\tau$ , a 90% C.L. bound  $E_\nu^2 dN_\nu/dE_\nu < 1.5_{-0.8}^{+0.5} 10^{-7} \text{ GeV cm}^{-2} \text{sr}^{-1} \text{s}^{-1}$  was derived in the energy range  $[2 \cdot 10^{17} - 5 \cdot 10^{19}] \text{ eV}$ . The sources of systematic uncertainties have been carefully addressed<sup>33</sup>; they are globally responsible for a factor of  $\sim 3$  uncertainty on the acceptance, which propagates to the final flux limit. Among them, physical quantities that have not been measured at those energies, such as the  $\nu$  cross-sections, the  $\tau$  polarization and energy losses, contribute resp.  $\sim 15\%$ ,  $\sim 30\%$  and  $\sim 40\%$ . The Monte Carlo simulations of the shower and the detector response add an extra  $\sim 25\%$  uncertainty, and the effect of neglecting the actual topology of the Auger site another  $\sim 18\%$ . As shown in Fig.4, Auger limit is nevertheless the best to date in the energy range where GZK neutrino fluxes (produced by the interaction of the observed UHECR with the cosmic microwave background) are likely to peak. To improve that limit by an order of magnitude or so will however require the accumulation of several more years of data.

## 6 Conclusions

The past three years have witnessed a phase of major development of the Southern Auger Observatory on the field, accompanied by a significant increase of the dataset. A lot of progress has been made in the understanding the detector, which resulted in a better control on the systematic uncertainties and in the development of reliable and robust analysis methods which allowed the release of first scientific results concerning the UHECR spectrum and angular distribution. If a continuation of the spectrum above  $10^{20}$  eV seems unlikely, a much larger data sample is still needed to determine the exact shape of the spectrum. Auger also sees a remarkably isotropic sky, except maybe at high energies where more data are necessary for a detailed study of clusterings and correlations, whatever the scale. Finally, Auger has already put competitive limits on the fluxes of UHE photons and neutrinos, thereby demonstrating its capabilities to work as a multi-messenger detector.

## Acknowledgments

The author wishes to thank both the organizers, for making so many fruitful exchanges between theorists and experimentalists possible, and the European Community 6<sup>th</sup> F.P. for supporting its activities in Auger through the Marie Curie Fellowship MEIF-CT-2005 025057.

## References

1. M. Takeda *et al.*, *Astropart. Phys.* **19** (2003) 447.
2. T. Abu-Zayyad *et al.* [HiRes Collaboration], *Astropart. Phys.* **23** (2005) 157.
3. A. M. Hillas, arXiv:astro-ph/0607109; D. F. Torres and L. A. Anchordoqui, *Rept. Prog. Phys.* **67** (2004) 1663; P. Bhattacharjee and G. Sigl, *Phys. Rept.* **327**, 109 (2000).
4. J. Abraham *et al.* [Pierre Auger Collaboration], *Nucl. Instrum. Meth. A* **523** (2004) 50.
5. D. Allard *et al.* [Pierre Auger Collaboration], *Proc. 29th ICRC* **7** (2005), 287.
6. C. Bonifazi *et al.* [Pierre Auger Collaboration], arXiv:0705.1856 [astro-ph].
7. P. Sommers [Pierre Auger Collaboration], *Proc. 29th ICRC* **7** (2005), 387.
8. M. Ave [Pierre Auger Collaboration], to appear in *Proc. 30th ICRC* (2007).
9. B. R. Dawson [Pierre Auger Collaboration], arXiv:0706.1105 [astro-ph].
10. M. Roth [Pierre Auger Collaboration], arXiv:0706.2096 [astro-ph].
11. T. Yamamoto [Pierre Auger Collaboration], to appear in *Proc. 30th ICRC* (2007).
12. G. Lefeuve *et al.*, arXiv:0704.1532 [astro-ph]; F. Arciprete *et al.*, *Nucl. Phys. Proc. Suppl.* **150** (2006) 186.
13. L. Perrone [Pierre Auger Collaboration], arXiv:0706.2643 [astro-ph].
14. D. Newton [Pierre Auger Collaboration], to appear in *Proc. 30th ICRC* (2007).
15. P. Facal San Luis [Pierre Auger Collaboration], to appear in *Proc. 30th ICRC* (2007).
16. N. Hayashida *et al.* [AGASA Collaboration], *Astropart. Phys.* **10** (1999) 303 ; M. Teshima *et al.* [AGASA Collaboration], *Proc. 27th ICRC* **1** (2001) 337.
17. J. A. Bellido *et al.*, *Astropart. Phys.* **15** (2001) 167.
18. F. Aharonian *et al.* [HESS Collaboration], *Astron. Astrophys.* **425** (2004) L13.
19. F. Aharonian *et al.* [HESS Collaboration], *Nature* **439** (2006) 695.
20. see e.g. G. Medina Tanco, A. Watson, *Proc. 27th ICRC* (2001) 531; R. Crocker *et al.*, *Astrophys. J.* **622** (2005) 273; F. Aharonian, A. Neronov, *astrophys. J.* **619** (2005) 306.
21. M. Aglietta *et al.* [Pierre Auger Collaboration], *Astropart. Phys.* **27** (2007) 244.
22. E.M. Santos [Pierre Auger Collaboration], arXiv:0706.2669 [astro-ph].
23. E. Armengaud [Pierre Auger Collaboration], arXiv:0706.2640 [astro-ph].
24. S. Mollerach [Pierre Auger Collaboration], arXiv:0706.1749 [astro-ph].
25. P. Tinyakov and I. Tkatchev, *JETP Lett.* **74** (2001) 445; D. Gorbunov *et al.*, *JETP Lett.* **80** (2004) 145; R. Abbasi *et al.* [HiRes Collaboration], *Astrophys. J.* **636** (2006) 680.
26. R. Clay [Pierre Auger Collaboration], *Proc. 28th ICRC* **1** (2003) 421.
27. L. D. Landau, I. Ya. Pomeranchuk Dokl. Akad. Nauk. SSSR **92** (1953), 535 & 735; A. B. Migdal, *Phys. Rev.* **103** (1956), 1811.
28. J. Abraham *et al.* [Pierre Auger Collaboration], *Astropart. Phys.* **27** (2007) 155.
29. M.D. Healy [Pierre Auger Collaboration], to appear in *Proc. 30th ICRC* (2007).
30. D. Fargion, *Astrophys. J.* **570** (2002) 909 and references therein.
31. X. Bertou *et al.*, *Astropart. Phys.* **17** (2002) 183.
32. J. Alvarez-Muñiz, [Pierre Auger Collaboration], to appear in *Proc. 30th ICRC* (2007).
33. O. B. Bigas [Pierre Auger Collaboration], arXiv:0706.1658 [astro-ph].